PCCP

Inelastic scattering in isotopologues of O_2–Ar: the effects of mass, symmetry, and density of states

Journal:	*Physical Chemistry Chemical Physics*
Manuscript ID	CP-ART-01-2021-000326.R1
Article Type:	Paper
Date Submitted by the Author:	23-Feb-2021

Complete List of Authors:	Bop, Cheikh; Université du Havre, LOMC Quintas-Sánchez, Ernesto; Missouri University of Science and Technology, Chemistry Sur, Sangeeta; Missouri University of Science and Technology, Chemistry Robin, Mathurin; Univ Le Havre Lique, François; Université du Havre, LOMC Dawes, Richard; Missouri University of Science and Technology, Chemistry

Journal Name

ARTICLE TYPE

Cite this: DOI: 10.1039/xxxxxxxxxx

Inelastic scattering in isotopologues of O_2–Ar: the effects of mass, symmetry, and density of states

Cheikh T. Bop,[a,b] Ernesto Quintas-Sánchez,[c] Sangeeta Sur,[c] Mathurin Robin,[a] François Lique,*[a,b] and Richard Dawes*[c]

Received Date
Accepted Date

DOI: 10.1039/xxxxxxxxxx

www.rsc.org/journalname

The two species considered here, O_2 (oxygen molecule) and Ar (argon-atom), are both abundant components of Earth's atmosphere and hence familiar collision partners in this medium. O_2 is quite reactive and extensively involved in atmospheric chemistry, including Chapman's cycle of the formation and destruction of ozone; while Ar, like N_2, typically plays the nevertheless crucial role of inert collider. Inert species can provide stabilization to metastable encounter-complexes through the energy transfer associated with inelastic collisions. The interplay of collision frequency and energy transfer efficiency, with state lifetimes and species concentrations, contributes to the rich and varied chemistry and dynamics found in diverse environments ranging from planetary atmospheres to the interstellar and circumstellar media. The nature and density of bound and resonance states, coupled electronic states, symmetry, and nuclear spin-statistics can all play a role. Here, we systematically investigate some of those factors by looking at the O_2–Ar system, comparing rigorous quantum-scattering calculations for the $^{16}O^{16}O$–^{40}Ar, $^{18}O^{16}O$–^{40}Ar, and $^{18}O^{18}O$–^{40}Ar isotope combinations. A new accurate potential energy surface was constructed for this purpose holding the O_2 bond distance at its vibrationally averaged distance.

1 Introduction

Inelastic scattering and the associated energy transfer play key roles in the stabilization dynamics of metastable encounter-complexes and hence govern the chemistry, as well as the energy flow and partitioning, in diverse environments ranging from planetary atmospheres to the interstellar and circumstellar media. A wide range of state lifetimes, species concentrations, collision frequencies and efficiencies, as well as radiative processes, all contribute to a rich dynamics, with many subtleties.

There are three stable isotopes of oxygen in the atmosphere: ^{16}O (99.76%), ^{17}O (0.038%) and ^{18}O (0.205%). Anomalous abundancies of the various isotopologues of ozone (O_3) were first detected in Earth's stratosphere in the 1980s,[1–3] with heavier species accumulating in greater concentration than expected from simple mass-dependent fractionation. This has been studied extensively,[4–22] and factors such as the nature and density of bound and resonance states, coupled electronic states, symmetry and nuclear spin-statistics—as well as photolysis steps in the Chapman's cycle of ozone formation/destruction—have all been investigated or implicated. It is a tremendous challenge to disentangle these effects accurately with appropriately rigorous quantum dynamics methods, given the complexity of ozone's coupled electronic structure, as well as the dimensionality of collision-complexes such as O_3–Ar, or the more atmospherically relevant O_3–N_2. The collisional stabilization relevant to ozone formation involves

[a] Laboratoire Ondes et Milieux Complexes, UMR 6294, Centre National de la Recherche Scientifique–Universite du Havre, F-76063 Le Havre, France.
[b] Universite du Rennes, CNRS, IPR (Institut de Physique de Rennes) - UMR 6251, F-35000 Rennes, France.
Email: francois.lique@univ-rennes1.fr; cheikhtidiane.bop@ucad.edu.sn
[c] Missouri University of Science and Technology, Rolla, MO 65409-0010, USA.
Email: dawesr@mst.edu, quintassancheze@mst.edu

highly excited resonance states of ozone (O_3^*).[23] Nevertheless, to explore some of the factors relating to collision efficiency, we previously performed bound states[24] and scattering[25] calculations for O_3–Ar with the ozone molecule in its ground rovibrational state, comparing results for $^{16}O^{16}O^{16}O$ with $^{16}O^{18}O^{16}O$ and $^{18}O^{16}O^{16}O$. One of the ^{18}O substitutions breaks the symmetry and roughly doubles the density of (boson) allowed states, while the other does not. Some models for energy transfer connect state density with transfer efficiency. For ozone, since the mass difference is small and the symmetry-breaking slight, it was found that the near evenness of the potential energy surface (PES) that is maintained, makes the cross-sections to the newly allowed states small, thus limiting their role. However, in the limited set of results that were obtained, there were still some tantalizing indications of slight differences for the broken-symmetry isotopologue. Rigorous quantum scattering calculations are computationally expensive for O_3–Ar and prohibit thoroughly exploring a wide variety of initial and final states. On the other hand, while not the subject of anomalous isotopic fractionation, the simpler O_2–Ar system offers a framework to explore some of the same issues, while also lending itself to more affordably extensive calculations, probing both excitation and de-excitation. Given an accurate PES, atom-diatom collision studies are quite routine and affordable.[26–28] The one complication encountered for the ground electronic state of molecular oxygen ($O_2(^3X_g^-)$) is that of the open-shell radical triplet spin-multiplicity and the consequent fine-structure splitting of the rotational level manifold. Lique and co-workers has previously reported a version of the close-coupling method implemented in `MOLSCAT`, modified to resolve scattering cross-sections to the individual fine-structure levels.[29–31]

The atmospherically relevant O_2–Ar system, has been the subject of both experimental and theoretical studies for several decades. As early as 1972, Tully and Lee[32] reported experimental differential cross section for O_2–Ar collisions at 73.9 meV average collision energy. One year later, Henderson and Ewing[33] reported the O_2–Ar infrared spectrum, making this system the first radical–rare gas complex to be observed spectroscopically; they also proposed a model potential, and concluded that the complex has a T-shaped equilibrium geometry. Since then, the O_2–Ar interaction has been explored extensively, both experimentally[32–47] and theoretically,[48–65] becoming a prototypical example of the interaction between a closed-shell atom and an open-shell molecule.

The experimental data providing valuable information about the inter-species potential for this complex, can be classified in three main groups: (*i*) differential[32,38,42] and integral[34–36] scattering cross sections, (*ii*) spectroscopic determinations,[33,40,42] and (*iii*) gaseous or condensed phase properties.[37,41,66] Several (semiempirical) PESs have been obtained through a combined analysis of as many data as possible from the different kinds of experiments.

Early estimates of the isotropic part of the intermolecular PES were done by Smith and Giraud[48] and Mingelgrin and Gordon[49]—by using earlier combination rules[67,68] and separate pure-species potentials.[69,70] The first anisotropic semiempirical potential was proposed by Pirani and Vecchiocattivi[50] through a multiproperty fit to experimental data, using as a parametric form a sophisticated highly-flexible function labeled ESMSV (exponential-spline-Morse-spline-vdW). The isotropic components of their PES was determined through a best fit to integral cross sections at thermal[34] and high energies,[35,36] the second virial coefficients,[71] the rainbow angle in the differential cross section,[32] and the P and R branches in the infrared absorption spectrum of the complex;[33] and the long-range anisotropies were determined by requiring the optimized potentials to reproduce an effective barrier for rotation of the O_2 molecule.[33] The short-range anisotropies were determined through the same procedure employed before by Mingelgrin and Gordonzo[49] and by Smith and Giraud,[48] approximating atom–diatom interactions as the scalar addition of the individual atom–atom interactions.[72] This PES was later used to study vibrationally inelastic processes,[51] the rotational predissociation of the complex,[55] and to calculate the low-temperature fine-structure and Zeeman spectrum;[52,53] although further examination found the (too small) well-depth as an obvious deficiency of the potential.[38] The ESMSV model was later improved—using a different functional form—by Candori *et al.*[54] to also reproduce the experimental total differential scattering cross section.[32,38] The new ESMSV model was further examined in a comparison with high-resolution molecular beam experiments.[42] Calculations showed the need for substantial corrections in the angular anisotropy of the interaction to correctly reproduce the experimental cross sections.[42,56] The model was also found to give only fair agreement with further experiments on pressure broadening cross sections.[39] The attractive well region of the O_2–Ar interaction potential was the subject of very detailed studies of the fine-structure spectrum and of the weak Zeeman splittings,[40] which also supplied suggestions for future improvements.

Later on, Gianturco and coworkers[57–60] proposed another set of improved semiempirical-PESs, labeled M3SV, which were aimed at a better reproduction of existing experimental data of transport properties (diffusion and viscosity)[41,66] and total differential cross sections

from crossed beam measurements.[42] Briefly, the M3SV model involved the selection of three different orientation-dependent Morse functions, which describe (respectively) the repulsive wall, the well region, and the attractive part of the well. Their best surface, Gianturco and Storozhev's PES,[60] proved to be more anisotropic than the ESMSV-PES, providing an improved description of the O_2–Ar interactions in the region of the global minimum, but was expected to be less accurate in the areas far from this region. In general, both ESMSV and M3SV empirical PES-models predict a moderately deep primary well for the system, located at the T-shaped configuration. Although this minimum is consistent with the equilibrium position for the complex reported in experimental studies,[33] the empirical models failed to reproduce one important aspect of the PES global topography: the existence of an additional (shallow) potential well for the linear configuration—which is consistently found in all subsequent *ab initio* calculations[61–63] and inferred from Coulomb explosion imaging experiments.[43]

The first attempt to construct a PES for the O_2–Ar system purely from *ab initio* calculations, in 1996, used coupled-cluster calculations to obtain the interaction energies only for linear and T-shaped geometries, and extrapolated the value of the potential for other geometries by interpolation (using a model that employs effective Ar–O potentials).[61] Although this PES exhibited two wells, with the one corresponding to the linear configuration being shallower, it represented the potential for intermediate bent geometries much less accurately. Cybulski and collaborators[62] obtained a more accurate *ab initio*-based PES, using supermolecular unrestricted Moller-Plesset perturbation theory[73] to compute the interaction energies for six different angular cuts (and eight intermolecular distances), fitting the *ab initio* data to an expansion of even Legendre polynomials and Morse-vdW functions[74]—this PES was used very recently by Wang and Carrington[64] for computing the rovibrational spectrum of the system. In 2004, the double-welled topology for the O_2–Ar PES was also confirmed by Naumkin and McCourt,[63] who used the restricted coupled-cluster RCCSD-T method[75,76] to compute the interaction energies for five equidistant angular cuts (and twelve intermolecular distances).

For this study, we develop a new highly-accurate PES, combining our automated interpolative PES-fitting approach with highly converged *ab initio* data. In Section 2 we describe the electronic structure method and fitting procedure, and characterize the PES. In Section 3 we describe the scattering calculations. In Section 4 we provide results and discussion, followed by our Conclusions and Outlook.

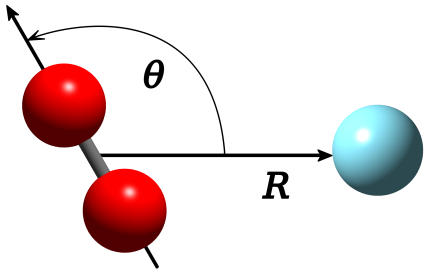

Fig. 1 Internal (Jacobi) coordinates used to describe the O_2–Ar interaction.

2 Potential energy surface

As illustrated in Figure 1, to describe the vdW interactions in the O_2–Ar complex we chose Jacobi coordinates. As can be seen in the figure, R is the length of the vector (*i.e.*, the distance) from the center-of-mass of the O_2 molecule to the argon atom, and θ corresponds to the angle between this vector and the O_2 bond axis.

The geometry of the O_2 molecule was held rigid at equilibrium, using the vibrationally averaged distance: r(O–O)$=1.20752$ Å, which is consistent with the experimental rotational constant.[77] Only a single PES was constructed, for the symmetric (*e.g.*, $^{16}O^{16}O$–Ar) complexes. Then, by transforming the coordinates to accommodate the shifted center-of-mass of the O_2 molecule upon isotopic substitution, the same PES could be used to study the broken symmetry case; this is very straightforward in 2D, with the oxygen molecule held rigid. Masses of 15.99491461957, 17.99915961286 and 39.9623831237 u were used for ^{16}O, ^{18}O and ^{40}Ar respectively. For the PES fitting data, the electronic energies were computed using explicitly-correlated unrestricted coupled-cluster theory[78] with all electrons (AE) correlated, extrapolated to the complete basis set limit, (AE)UCCSD(T)-F12b/CBS. The basis extrapolation was performed using the Peterson CVTZ-F12 and CVQZ-F12 bases[79] and the l^{-3} formula.[80] All *ab initio* calculations were performed using the `MOLPRO` electronic structure code package.[81] Stable convergence to the roHF reference was achieved by first using `MOLPRO`'s CASSCF (multi) algorithm with the occupation of the desired configuration specified, followed by a single iteration of the restricted open HF (roHF) SCF algorithm to prepare the orbitals for the UCCSD(T)-F12b procedure. A *geminal beta* coefficient value of 1.5 was specified for the all-electron F12 calculations. Some additional benchmarking of the computed well-depth was performed comparing the standard UCCSD(T) and explicitly correlated UCCSD(T)-F12b methods, comparing also valence-only, and all-electron (core) correlation. The results are given in Table 1. As can be seen in the table, the well-depth at the CBS level consid-

Table 1 Calculated well-depth for the T-shaped global minimum ($R = 3.5385$ Å and $\theta = 90$ degrees), comparing standard and explicitly-correlated unrestricted coupled-cluster theory. The effect of including the core electrons in the correlation treatment (AE) is also compared. Energy values are in cm^{-1}

n	VnZ-F12 UCCSD(T)-F12b	CVnZ-F12 (AE)UCCSD(T)-F12b
2	125.5	83.0
3	116.4	99.3
4	111.1	100.9
5	113.3	—
CBS*	116.9	100.7
n	aug-cc-pVnZ UCCSD(T)	aug-cc-pCVnZ (AE)UCCSD(T)
2	128.1	146.1
3	126.2	128.9
4	123.4	122.8
5	120.4	118.1
CBS*	114.8	107.9

* CBS values were obtained using the three highest available zeta values for each method and basis series, and an optimized power-law formula. The well-depth on the fitted PES is 101.6 cm^{-1}.

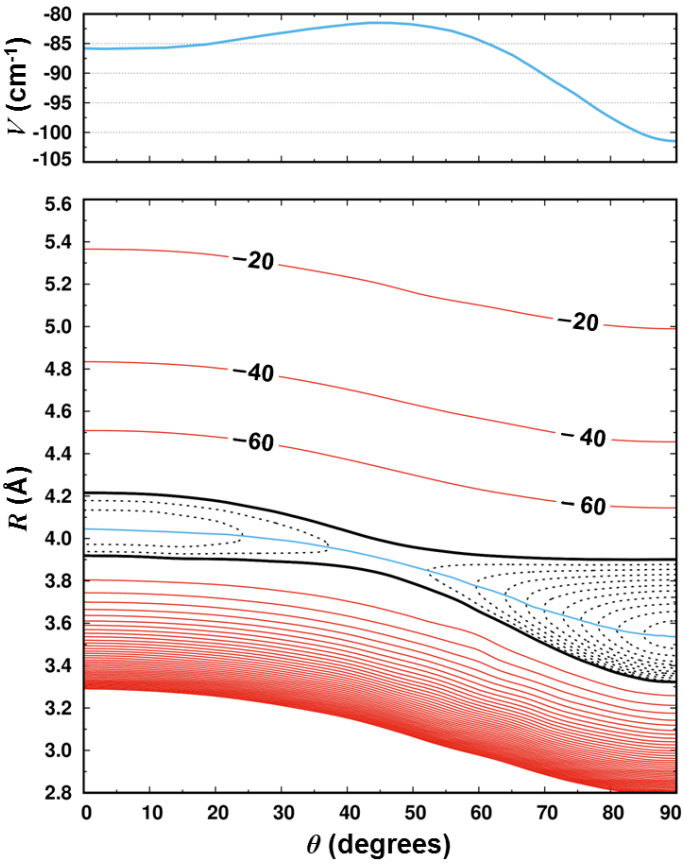

Fig. 2 Lower panel: 2D plot of the PES. The black contour represents the energy $E_0 = -80$ cm^{-1}. Dashed (solid) contours represents energies below (above) E_0, in steps of 2 cm^{-1} (20 cm^{-1}). The continuous blue line represents the minimum energy path connecting the two minima. Upper panel: Energies along the minimum energy path between the minima.

ering only valence electron-correlation is quite consistent for both the standard and explicitly-correlated methods: 115 cm^{-1} and 117 cm^{-1} respectively. Inclusion of core electrons in the correlation treatment reduces the well-depth fairly significantly, to 108 cm^{-1} and 101 cm^{-1} for the standard and explicitly correlated methods respectively. The 7 cm^{-1} difference between methods at the CBS level is slightly unusual (somewhat larger than typical). Similar behavior was noted in an earlier study of the CO dimer.[82] Since the extrapolation beyond the highest zeta level is much less for the F12 method, and is hence perhaps more reliable, it was chosen for the PES construction. Indeed, this approach was found to be more accurate for the CO dimer.

The two dimensional (2D) PES was constructed using an automated interpolating moving least squares (IMLS) methodology, which has been used in several previous studies[24,83–87] and has been recently released as a software package under the name AUTOSURF.[88] As usual,[89] a local fit was expanded about each data point and the final potential is obtained as the normalized weighted sum of the local fits. This interpolative approach can accommodate arbitrary energy-surface topographies and is particularly advantageous in cases of PESs with large anisotropy, which are challenging for traditional quadrature-type expansions. The procedure has been described in detail elsewhere.[88–91] The shortest intermonomer center-of-mass distance considered is $R = 2.5$ Å, with the additional restriction of a maximum repulsive energy of 6 kcal/mol (~ 2100 cm^{-1}) above the separated monomers asymptote. The *ab initio* data coverage in the fitted PES extends to $R = 15.0$ Å. Taking advantage of the system's symmetry, energies are only computed in the reduced angular range $0 < \theta < 90$ degrees. For the final PES, the global root-mean-squared fitting error was 0.24 cm^{-1} (0.01 cm^{-1} for energy-regions below the asympote) and the total number of automatically generated symmetry-unique points needed to reach that target was 210. The analytical representation of the PES is available from the authors upon request.

A contour plot of the PES is given in Figure 2 (lower panel). As can be seen in the figure, the global minimum occurs for the T-shaped geometry, with an equilibrium distance on the fitted PES at $R = 3.539$ Å. Somewhat similar distances of $R = 3.58$, 3.55, and 3.48 Å were reported in references 60, 62, and 63 respectively. There is also a local collinear minimum at $R = 4.045$ Å. We note that although—as discussed above and given in Table 1—the well-depth

Table 2 Geometric parameters and potential energy for the global (GM) and local (LM) minima, as well as the transition structure (TS) of the O_2–Ar complex. All energies are given relative to the asymptote. Distances are in Angströms, angles are in degrees, and energies are in cm^{-1}

	GM	LM	TS
R	3.539	4.044	3.952
θ	90.00	0.00	38.34
V	-101.49	-85.83	-82.00

for standard UCCSD(T)/CBS without core-electron correlation is slightly deeper, the equilibrium geometric parameters are very similar at $R = 3.541$ Å and $R = 4.049$ Å for the global and local minima respectively. On the PES, passage from the global minimum to the local collinear minimum involves surmounting a barrier of about 20 cm^{-1}. The upper panel in Figure 2 illustrates the minimum energy path between minima. The energies and geometric parameters of the minima are given in Table 2.

3 Scattering calculations

In this work, we focus on the rotational (de)excitation of $^{16}O^{16}O$, $^{16}O^{18}O$ and $^{18}O^{18}O$ (hereafter denoted as 66, 68 and 88, respectively) induced by collision with Ar. As the ground electronic state of the targets is a $^3\Sigma^-$ state, the rotational levels are split into fine structure levels due to the spin-rotation coupling.[92] Considering the intermediate coupling scheme, the wave function describing the rotation of the (66, 68 and 88) oxygen molecule can be expressed for $j \geq 1$ as:[93]

$$
\begin{aligned}
|F_1 jm\rangle &= \cos\alpha\,|N = j-1, Sjm\rangle + \sin\alpha\,|N = j+1, Sjm\rangle \\
|F_2 jm\rangle &= |N = j, Sjm\rangle \\
|F_3 jm\rangle &= \cos\alpha\,|N = j+1, Sjm\rangle - \sin\alpha\,|N = j-1, Sjm\rangle \quad (1)
\end{aligned}
$$

with $|N, Sjm\rangle$ being the Hund's case (b) basis functions and the total angular momentum of the molecule (j) being defined as a sum of the nuclear rotational quantum number (N) and the electronic spin (S) angular momenta:[93,94] $j = N + S$. The mixing angle (α) is determined by diagonalizing the molecular Hamiltonian. In the pure Hund's case (b) limit (α tends to zero) the values $N = j-1$, $N = j$, and $N = j+1$, as shown in equation 1, correspond to the spectroscopic indexes F_1, F_2, and F_3, respectively. The value of α was found to be very small and hence hereafter, we will use the pure Hund's case (b) limit notation for the energy levels even though the intermediate coupling scheme was explicitly considered in the calculations.

Rotational energy diagrams for the ground vibrational

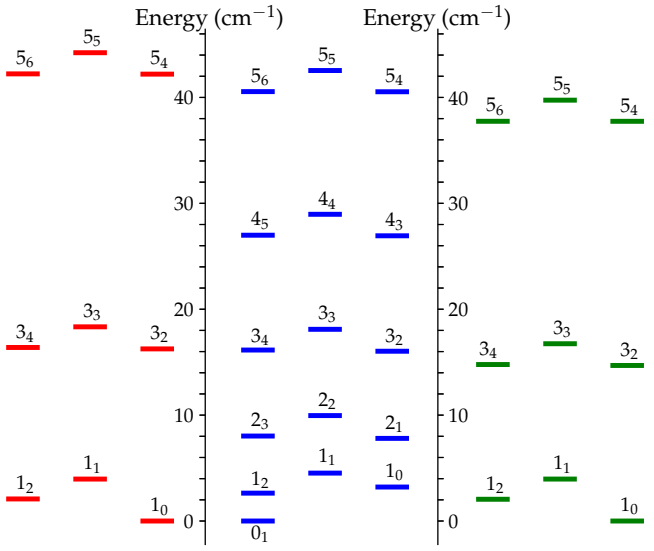

Fig. 3 Rotational energy levels below 50 cm^{-1} for the 66 (red), 68 (blue) and 88 (green) isotopologues of molecular oxygen. The energy levels are labeled as N_j. For each isotopologue, the levels are separated in three columns, corresponding to the spectroscopic indexes F_1 (left), F_2 (center), and F_3 (right). See the text for details.

state of all (66, 68 and 88) isotopologues of O_2 are shown in Fig. 3 for N_j levels up to $N = 5$. Since ^{16}O and ^{18}O are spin-zero bosons, for the 66 and 88 homonuclear isotopologues the quantum number N is restricted to have odd values, while this restriction does not exist for the 68 oxygen molecule; thus the density of states is roughly doubled for the 68 isotopologue. In tabulating detailed state-to-state results, we treated transitions between levels up to $N = 21$, which includes the lowest 33 fine-structure levels for the 66 and 88 isotopologues, and 64 levels for the 68 isotopologue. One can also notice a more subtle increase in state density—caused by the slight change (decrease) in the rotational constant of the oxygen molecule when the mass of the system increases—going from 66 to 68 to 88.

In each isotopologue, considering fine-structure levels well below the first excited vibrational state, the gaps between the groups of states for each N increase. This sparseness in the state-manifold (in this energy range) is in contrast to the distribution of states in the energy-range relevant to the stabilization of ozone, where the density of (bound) vibrational states, and hence ro-vibrational states, increases and is much higher towards the top of the well.[95] In ozone, the density of resonances above dissociation is less and each state is associated with a lifetime. Stabilization of ozone involves de-excitation from an unbound resonance state, just above the dissociation threshold, into the denser manifold of bound ro-vibrational states below.

Scattering calculations were carried out using the exact

close-coupling quantum mechanical method for total energies (E) up to 2000 cm^{-1}. In practice, the coupled equations were solved in the intermediate coupling scheme, as implemented in the modified MOLSCAT code,[96] in order to resolve the fine structure of the isotopologues. Given the relatively low cost of the calculations, parameters were tested and selected generously to ensure good convergence. The radial wave function was propagated from 2 Å to at least 60 Å using the modified log derivative-airy integrator.[97] The integration step was kept below 0.1 Å by setting the STEPS-parameter to 30 for total energies below 100 cm^{-1} and gradually decreasing this variable down to 6 for 1500 cm$^{-1} \leq E \leq$ 2000 cm^{-1}. In order to take into account the coupling between closed and open channels, we included in the rotational basis of the isotopologues all accessible levels along with at least nine energetically closed channels. Typically, for the spin-zero bosons N was smoothly increased from 11 (for energies below 30 cm^{-1}) to 33 (for 1500 cm$^{-1} \leq E \leq$ 2000 cm^{-1}). In the case of the 68 isotopologue, incrementing by one the above N-values was enough to converge the cross-sections. Considering these basic inputs, we spanned the total energy using an irregular step. More explicitly, the spacing was set to 1 cm^{-1} for $E \leq$ 800 cm^{-1}, 5 cm^{-1} for 805 cm$^{-1} \leq E \leq$ 900 cm^{-1}, 10 cm^{-1} for 910 cm$^{-1} \leq E \leq$ 1000 cm^{-1} and 20 cm^{-1} for 1020 cm$^{-1} \leq E \leq$ 2000 cm^{-1}. The energy grid used below 800 cm^{-1} is small enough to describe fairly well the resonances which are expected at low kinetic energy.

Because the quantum scattering calculations require a particular expansion of the angular dependence of the PES, the 2D IMLS potential was expressed in the form:

$$V(R,\theta) = \sum_{\lambda} V_{\lambda}(R) P_{\lambda}(\cos\,\theta) \qquad (2)$$

where coefficients V_{λ} only depend on coordinate R and $P_{\lambda}(\cos\,\theta)$ is the Legendre polynomial of order λ. Terms up to $\lambda_{\max} = 18$ were retained in the polynomial expansion of the potential providing a representation with negligible fitting error.

Using the computational scheme described above, the inelastic cross-sections (σ) associated with transitions from each initial rotational state N_j to each final state $N'_{j'}$ were obtained at each kinetic energy E_k ($E_k = E - E_{N_j}$), and then thermally averaged using the Maxwell-Boltzmann velocity distribution to derive fine-structure resolved rate coefficients (k) for temperatures (T) ranging up to 200 K:

$$k_{N_j \to N'_{j'}}(T) = \left(\frac{8}{\pi\mu\beta}\right)^{1/2} \beta^2 \int_0^{\infty} E_k \sigma_{N_j \to N'_{j'}}(E_k) e^{-\beta E_k}\, dE_k \qquad (3)$$

The parameter β is defined as $1/k_{\mathrm{B}}T$, with k_{B} being the

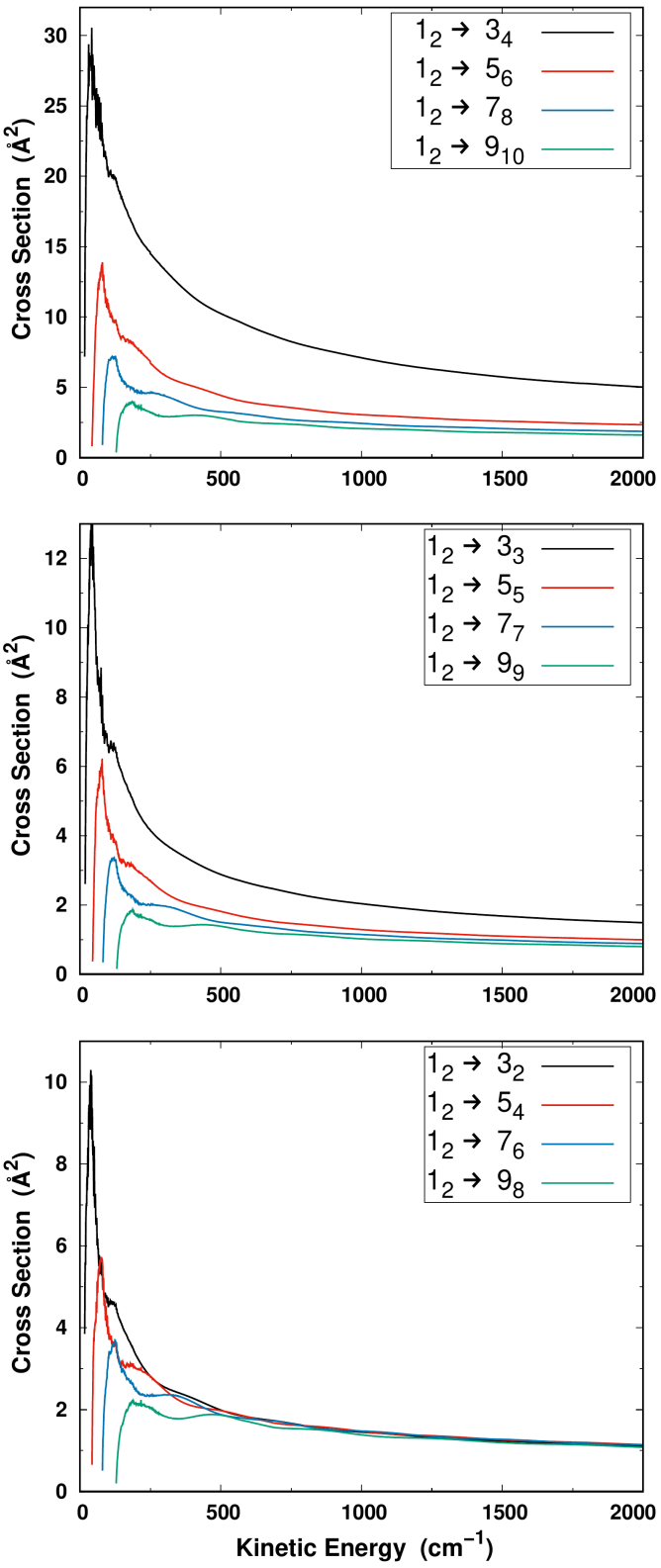

Fig. 4 Collisional excitation cross sections from the $N_j = 1_2$ initial state for the 66 isotopologue as a function of collision energy. The first few F-preserving (upper panel) and F-changing excitations (two lower panels) are plotted.

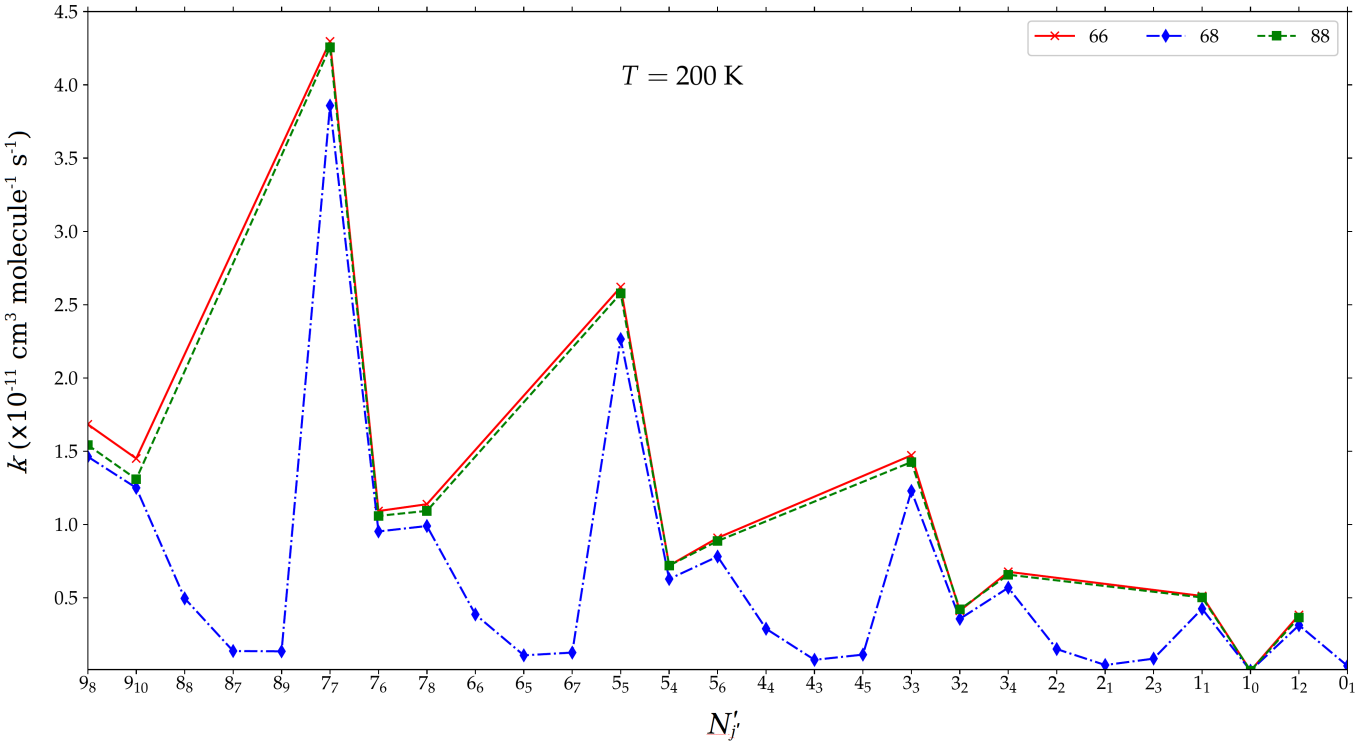

Fig. 5 State-to-state downward rate coefficients for the 66, 68 and 88 isotopologues of molecular oxygen induced by collision of a particular initially excited state (the $N_j = 9_9$ F_2-state) with argon at $T = 200$ K. Transitions among fine structure levels are labeled as $(N_j = 9_9) \rightarrow N'_{j'}$.

Boltzmann constant, and μ stands for the reduced mass of the system.

4 Results and discussion

In 2010, Lique reported[98] the fine-structure-resolved rates for excitation of ^{16}O^{16}O by collision with helium, considering mainly transitions from the $N_j = 1_2$ (F_1) initial state. Two main propensities were observed: a) the expected drop in cross-sections and corresponding rates with increasing ΔN, and b) significant favoring of $\Delta j = \Delta N$ (F-preserving) transitions. Shape and Feshbach resonances were observed in the lowest energy region of the cross-section plots, extending to about 125 cm^{-1}, well past the well-depth of about 28 cm^{-1} in the ^{16}O^{16}O–He system. Here, with argon as the collision partner, the masses of the two colliders are much more similar, and the well-depth is roughly four times greater. Correspondingly, the resonances seen in the low-energy part of Figure 4 extend to about 250 cm^{-1}, only slightly more than double the well-depth. Before exploring the effects of isotopic substitution on quenching (de-excitation) rates, we first tested the effects of mass and well-depth on the scattering cross sections by comparing the same excitation transitions from $N, F_i = 1, F_1$ as given in Figure 1 of Ref. 98, but replacing helium with argon. The excitation cross sections for the 66 isotopologue—from the $N, F_i = 1, F_1$ initial state—is shown in Figure 4 as a function of collision energy. The propensities are qualitatively similar to those computed for the helium collider, but with the cross sections somewhat larger and the resonance structure extending to higher energies, consistent with the greater well-depth as expected. The $\Delta j = \Delta N$ propensity is still observed, but not as significantly—the $\Delta j \neq \Delta N$ (F-changing) cross sections are relatively larger for argon compared to helium. This effect can be attributed to the larger well-depth in the PES that allows the spin projection to change more easily.

Next, to explore the effects of isotopic substitution on quenching of initially excited states, rates of de-excitation are plotted in Figure 5 (at 200 K) for the $N_j = 9_9$ F_2-state to all lower states. For the two symmetric systems, 66 and 88, the rates decrease with increasing ΔN and significantly favor the $\Delta j = \Delta N$ transitions from the initial state with $N = j$. For the 68 system, in addition to a similar pattern of rate coefficients for $\Delta N = even$ transitions (but slightly reduced), weaker $\Delta N = odd$ transitions to the even-N states arise which are not available in the 66 and 88 systems (since those corresponding states do not exist, see Figure 3). For 68, within the weaker odd ΔN transitions to

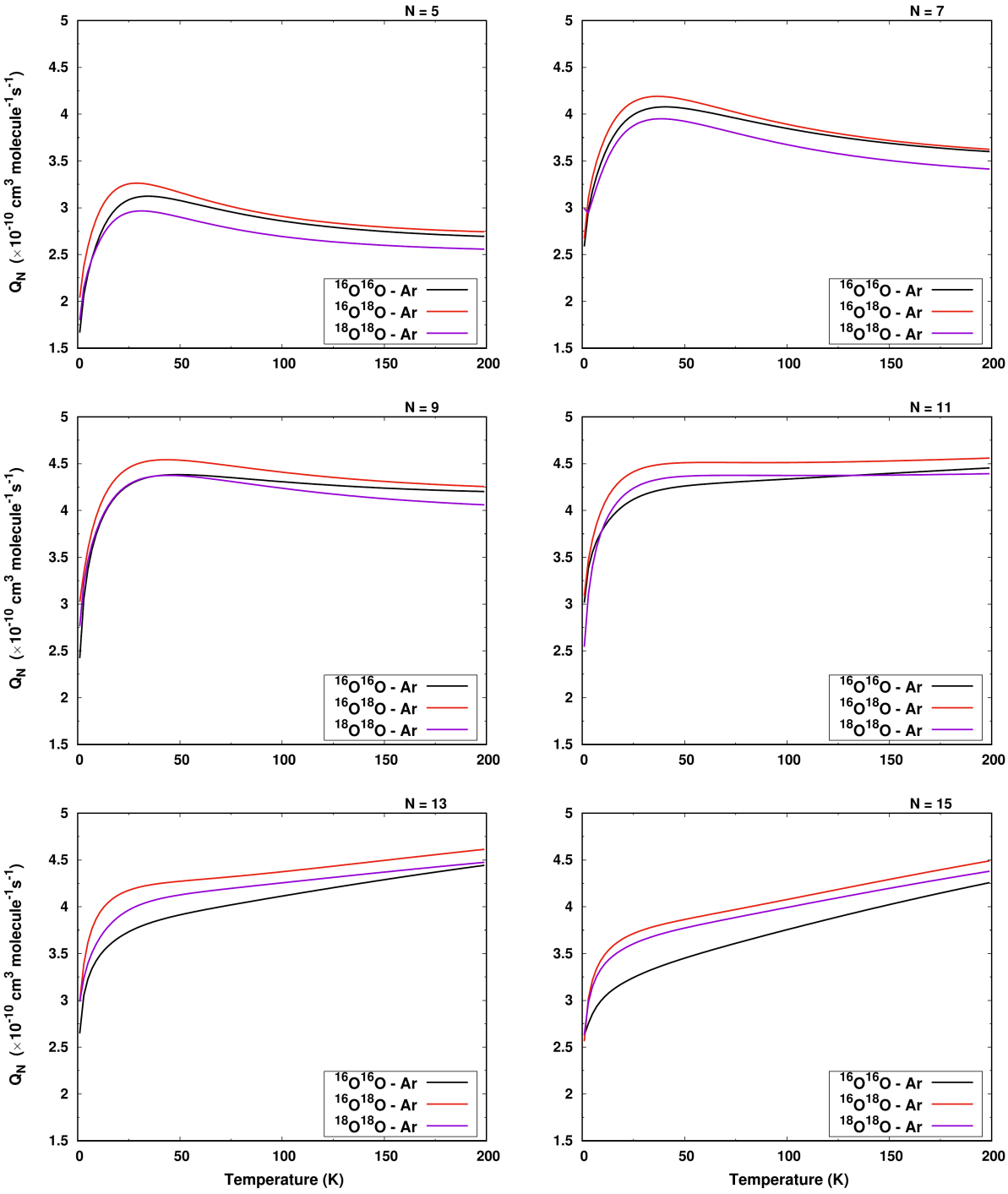

Fig. 6 Cumulative de-excitation rates Q_N (defined in Eqn. 4) from initial states with $N = 5$ (upper left), $N = 7$ (upper right), $N = 9$ (middle left), $N = 11$ (middle right), $N = 13$ (lower left), $N = 15$ (lower right), for all (66, 68 and 88) isotopologues of oxygen, as a function of temperature.

the even-N states, similar patterns of decreasing rates with increasing ΔN and favoring of $\Delta j = \Delta N$ transitions are also found.

The atmospherically relevant question regarding stabilization of ozone in the stratosphere—upon symmetry breaking via isotopic substitution—is whether the net contribution of de-excitation rate coefficients to the newly allowed states in the symmetry-broken systems is greater than any reduction in rates to the existing manifold of states in the symmetric systems. Differences in the isotopo-

logues' scattering dynamics arise due to different energy level structures, different reduced masses, and the symmetry breaking of the PES for the 68 isotope.

We therefore define a quenching function $Q_N(T)$, which for each system and a given N combines the rates of de-excitation to all lower energy states:

$$Q_N(T) = \sum_{j,N',j'} k_{N_j \to N'_{j'}}(T) \quad (4)$$

where we combine the three fine-level contributions, since the clusters of energies are well-characterized by N and this splitting is not found in (singlet) ozone molecules. Looking for example at the three states with $N = 5$ for the 66 isotopologue, in the upper left panel of Figure 3, $Q_5(T)$ is evaluated by combining the rates for each of the three $N = 5$ states in transitions to all of the $N = 3$ and $N = 1$ states below. $Q_N(T)$ is evaluated the same way for the 68 and 88 systems except that for 68, there are additional contributions from transitions to the $N = even$ states.

In Figure 6, $Q_N(T)$ is plotted for $N = 5$, 7, 9, 11, 13 and 15. For each increasing N, which represents higher energy and sparser state manifolds, the total rate of collisional quenching is consistently higher for the symmetry-broken 68 isotopologue over the entire temperature range. The quenching rate coefficients for 66 and 88 undergo some crossings as a function of temperature due to the interplay of the different reduced masses of the collision systems, and the slightly denser manifold of states for 88 compared with 66 (*cf.* Figure 3).

There is an interesting aspect to the dynamics of this and other diatomic species in their ground vibrational state (although less relevant to systems, such as ozone, in their dense manifold of rovibrational states near dissociation). Here, as we consider quenching for increasing N, the function $Q_N(T)$ includes summation over an increasing number of states below. However, those states, even the nearest ones, are found further and further away in energy. Thus, as seen in Figure 6, the magnitude of $Q_N(T)$ increases significantly going from $N = 5$ to $N = 7$, but then starts to level off toward $N = 11$. Indeed, $Q_N(T)$ starts to drop for $N = 13$ and $N = 15$ (at least at low temperatures) as the gaps to even the closest states widen.

To explore the relative enhancement or reduction in quenching rates upon isotopic substitution in the parent $^{16}O^{16}O$ molecule (denoted 66), Figure 7 shows the percentage change in quenching rates relative to that of the 66 system over the complete temperature range. The relative enhancement for the 68 system over 66 is not obvious in Figure 6, although it is clear that the rate coefficients are larger throughout. In Figure 7, for $N = 5$ (upper left panel), the enhancement is seen to be largest (about 15 percent) at the lowest temperatures, before dropping and leveling off at about 2 percent for temperatures above 100 K. The relative rate for 88 at $N = 5$ is enhanced at very low temperatures, but it drops, crossing the 66 result, thus exhibiting a roughly 5 percent reduction for most of the temperature range. For various N there are subtleties in the enhancement of 88 relative to 66, for example being found below 66 at $N = 7$ over the entire temperature range, but above it for $N = 13$ and $N = 15$. Symmetry-broken 68 is enhanced relative to 66 for all of the N considered (and is larger than 88 also), but as seen in Figure 7 the percentage enhancement is smallest for $N = 7$, before increasing significantly with N, ranging from 5 to 15 percent across the temperature range for $N = 15$.

5 Conclusions and Outlook

We report a new highly accurate PES for the O_2–Ar collision system based on interpolated energies calculated using explicitly-correlated (including all electrons) coupled-cluster theory extrapolated to the complete basis limit. The PES was used to study scattering processes for three isotopologues of O_2 ($^{16}O^{16}O$, $^{18}O^{18}O$, and $^{16}O^{18}O$) colliding with argon atoms using the rigorous close-coupling formalism. A large set of fine-structure-resolved state-to-state cross sections and rates were determined.

Motivated by anomalous abundancies of certain heavy isotopologues of ozone found in the stratosphere, the results provide insight into the effects of slight mass changes upon isotopic substitution, but also more dramatically, the roughly doubling of the density of states for symmetry broken isotopologues ($^{16}O^{18}O$ in this study). Due to the PES being either even ($^{16}O^{16}O$ and $^{18}O^{18}O$) or nearly so ($^{16}O^{18}O$), the strongest transitions are for $\Delta N = even$ and drop with increasing ΔN. The propensity for $\Delta j = \Delta N$ (F-preserving) transitions was also observed, similar to that reported in a previous study of excitation of O_2 by helium. Here, a major focus was on the effects of isotopic substitution on collisional stabilization (quenching). Remarkably, the symmetry-broken $^{16}O^{18}O$ system was found to consistently exhibit enhanced quenching relative to the parent $^{16}O^{16}O$ system over the studied range of temperatures. Since the symmetry breaking is slight, transitions to the newly allowed states are relatively weak. Nevertheless, the net result is enhanced quenching on the order of 2-15 percent depending on the temperature and initial state energies.

6 Acknowledgments

R.D. is supported by the U.S. Department of Energy, Office of Science, Office of Basic Energy Sciences (Award

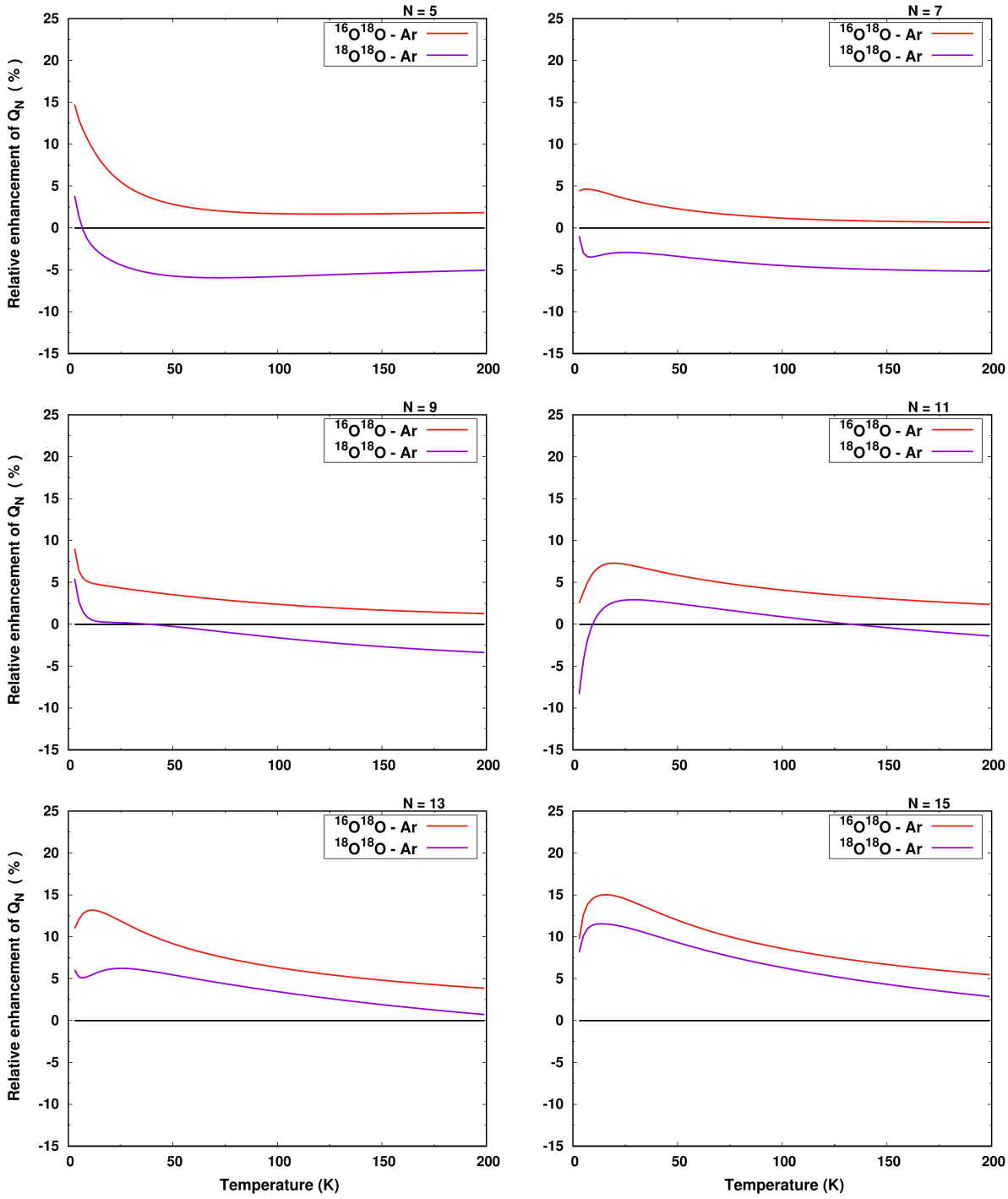

Fig. 7 Relative enhancement of $Q_N(T)$ upon isotopic substitution compared to $^{16}O^{16}O$, (see Figure 6 and text) from initial states with N = 5 (upper left), N = 7 (upper right), $N = 9$ (middle left), $N = 11$ (middle right), $N = 13$ (lower left), $N = 15$ (lower right), for all (66, 68 and 88) isotopologues of oxygen, as a function of temperature.

DE-SC0019740). R.D. thanks Paul Dagdigian for insightful suggestions. F.L., M.R., and C.T.B. acknowledge financial support from the European Research Council (Consolidator Grant COLLEXISM, grant agreement 811363), the Institut Universitaire de France, and the Programme National "Physique et Chimie du Milieu Interstellaire" (PCMI) of CNRS/INSU with INC/INP, co-funded by CEA and CNES. We wish to acknowledge the support from the CINES/GENCI for awarding us access to the OCCIGEN supercomputer within the A0090411036 project.

Notes and references

1 K. Mauersberger, *Geophysical Research Letters*, 1981, **8**, 935–937.

2 M. H. Thiemens and J. E. Heidenreich, *Science*, 1983, **219**, 1073–1075.

3 K. Mauersberger, *Geophysical Research Letters*, 1987, **14**, 80–83.

4 M. Quack, *Molecular Physics*, 1977, **34**, 477–504.

5 J. E. Heidenreich III and M. H. Thiemens, *The Journal of chemical physics*, 1986, **84**, 2129–2136.

6 J. Guenther, D. Krankowsky and K. Mauersberger, *Chemical Physics Letters*, 2000, **324**, 31–36.

7 B. Hathorn and R. Marcus, *The Journal of Chemical Physics*, 2000, **113**, 9497–9509.

8 K. Mauersberger, P. Lämmerzahl and D. Krankowsky, *Geophysical Research Letters*, 2001, **28**, 3155–3158.

9 Y. Q. Gao and R. Marcus, *Science*, 2001, **293**, 259–263.

10 Y. Q. Gao and R. Marcus, *The Journal of chemical physics*, 2002, **116**, 137–154.

11 Y. Q. Gao, W.-C. Chen and R. Marcus, *The Journal of chemical physics*, 2002, **117**, 1536–1543.

12 S. Chakraborty and S. Bhattacharya, *The Journal of chemical physics*, 2003, **118**, 2164–2172.

13 D. Babikov, B. K. Kendrick, R. B. Walker, R. T Pack, P. Fleurat-Lesard and R. Schinke, *The Journal of chemical physics*, 2003, **118**, 6298–6308.

14 D. Babikov, B. Kendrick, R. Walker, R. Schinke and R. Pack, *Chemical physics letters*, 2003, **372**, 686–691.

15 D. Babikov, B. K. Kendrick, R. B. Walker, R. T Pack, P. Fleurat-Lesard and R. Schinke, *The Journal of chemical physics*, 2003, **119**, 2577–2589.

16 V. Haverd, G. C. Toon and D. W. Griffith, *Geophysical research letters*, 2005, **32**, L22808.

17 A. S. Cole and K. A. Boering, *The Journal of chemical physics*, 2006, **125**, 184301.

18 M.-C. Liang, F. W. Irion, J. D. Weibel, C. E. Miller, G. A. Blake and Y. L. Yung, *Journal of Geophysical Research: Atmospheres*, 2006, **111**, D02302.

19 D. Krankowsky, P. Lämmerzahl, K. Mauersberger, C. Janssen, B. Tuzson and T. Röckmann, *Journal of Geophysical Research: Atmospheres*, 2007, **112**, D08301.

20 S. Ndengué, S. Madronich, F. Gatti, H.-D. Meyer, O. Motapon and R. Jost, *Journal of Geophysical Research: Atmospheres*, 2014, **119**, 4286–4302.

21 T. Sato, K. Kuribayashi, N. Yoshida and Y. Kasai, *Geophysical Research Letters*, 2017, **44**, 6399–6406.

22 A. Teplukhin and D. Babikov, *The Journal of Physical Chemistry A*, 2018, **122**, 9177–9190.

23 Z. Sun, D. Yu, W. Xie, J. Hou, R. Dawes and H. Guo, *The Journal of Chemical Physics*, 2015, **142**, 174312.

24 S. Sur, E. Quintas-Sánchez, S. A. Ndengué and R. Dawes, *Physical Chemistry Chemical Physics*, 2019, **21**, 9168–9180.

25 S. Sur, S. A. Ndengué, E. Quintas-Sánchez, C. Bop, F. Lique and R. Dawes, *Physical Chemistry Chemical Physics*, 2020, **22**, 1869–1880.

26 D. Manolopoulos, *The Journal of chemical physics*, 1986, **85**, 6425–6429.

27 J. M. Hutson and C. R. Le Sueur, *Computer Physics Communications*, 2019, **241**, 9–18.

28 S. Ndengué, R. Dawes, F. Gatti and H. Guo, *The Journal of Physical Chemistry A*, 2018, **122**, 6381–6390.

29 F. Dumouchel, J. Kłos, R. Toboła, A. Bacmann, S. Maret, P. Hily-Blant, A. Faure and F. Lique, *The Journal of Chemical Physics*, 2012, **137**, 114306.

30 C. K. Bishwakarma, G. van Oevelen, R. Scheidsbach, D. H. Parker, Y. Kalugina and F. Lique, *The Journal of Physical Chemistry A*, 2016, **120**, 868–874.

31 K. M. Walker, F. Lique and R. Dawes, *Monthly Notices of the Royal Astronomical Society*, 2018, **473**, 1407–1415.

32 F. P. Tully and Y. T. Lee, *The Journal of Chemical Physics*, 1972, **57**, 866–869.

33 G. Henderson and G. E. Ewing, *The Journal of Chemical Physics*, 1973, **59**, 2280–2293.

34 E. Luzzatti, F. Pirani and F. Vecchiocattivi, *Molecular Physics*, 1977, **34**, 1279–1286.

35 Y. N. Belyaev and V. Leonas, *Soviet Physics Doklady*, 1967, **11**, 866.

36 J. E. Jordan, S. O. Colgate, I. Amdur and E. A. Mason, *The Journal of Chemical Physics*, 1970, **52**, 1143–1149.

37 B. J. Setzer and H. M. Pickett, *The Journal of Chemical Physics*, 1977, **67**, 340–343.

38 G. Rotzoll, *Chemical Physics Letters*, 1982, **88**, 179–184.

39 G. C. Corey and F. R. McCourt, *The Journal of Chemical Physics*, 1984, **81**, 3892–3907.

40 J. Mettes, B. Heymen, P. Verhoeve, J. Reuss, D. Lainé and G. Brocks, *Chemical Physics*, 1985, **92**, 9–23.

41 R. Trengove, K. Harris, H. Robjohns and P. J. Dunlop, *Physica A: Statistical Mechanics and its Applications*, 1985, **131**, 506–519.

42 M. Faubel and G. Kraft, *The Journal of Chemical Physics*, 1986, **85**, 2671–2683.

43 J. Wu, M. Kunitski, L. P. H. Schmidt, T. Jahnke and R. Dörner, *The Journal of Chemical Physics*, 2012, **137**, 104308.

44 M. Camac, *The Journal of Chemical Physics*, 1961, **34**, 448–459.

45 M. Ukai, K. Kameta, K. Shinsaka, Y. Hatano, T. Hi-

rayama, S.-i. Nagaoka and K. Kimura, *Chemical Physics Letters*, 1990, **167**, 334–340.

46 D. Herrick, M. Robin and A. Gedanken, *Journal of Molecular Spectroscopy*, 1989, **133**, 61–81.

47 K. G. Owen, D. F. Davidson and R. K. Hanson, *Journal of Thermophysics and Heat Transfer*, 2016, **30**, 791–798.

48 E. W. Smith and M. Giraud, *The Journal of Chemical Physics*, 1979, **71**, 4209–4217.

49 U. Mingelgrin and R. G. Gordon, *The Journal of Chemical Physics*, 1979, **70**, 3828–3839.

50 F. Pirani and F. Vecchiocattivi, *Chemical Physics*, 1981, **59**, 387–396.

51 F. Battaglia, F. A. Gianturco, P. Casavecchia, F. Pirani and F. Vecchiocattivi, *Faraday Discuss. Chem. Soc.*, 1982, **73**, 257–273.

52 J. Tennyson and J. Mettes, *Chemical Physics*, 1983, **76**, 195–202.

53 A. van der Avoird, *The Journal of Chemical Physics*, 1983, **79**, 1170–1175.

54 R. Candori, F. Pirani and F. Vecchiocattivi, *Chemical Physics Letters*, 1983, **102**, 412–415.

55 C. Serrano, O. Roncero, P. Mareca, P. Villarreal and G. Delgado-Barrio, *Chemical Physics*, 1985, **92**, 155–162.

56 M. S. Bowers, M. Faubel and K. T. Tang, *The Journal of Chemical Physics*, 1987, **87**, 5687–5693.

57 F. A. Gianturco and A. Palma, *Intramolecular Dynamics. The Jerusalem Symposia on Quantum Chemistry and Biochemistry, vol 15*, Springer, Dordrecht, 1982, ch. 5, pp. 63–87.

58 M. Faubel, K. H. Kohl, J. P. Toennies and F. A. Gianturco, *The Journal of Chemical Physics*, 1983, **78**, 5629–5636.

59 F. Gianturco, M. Venanzi and A. Dickinson, *Molecular Physics*, 1988, **65**, 585–598.

60 F. A. Gianturco and A. Storozhev, *The Journal of Chemical Physics*, 1994, **101**, 9624–9634.

61 F. Naumkin and P. Knowles, *FEMTOCHEMISTRY–Ultrafast Chemical and Physical Processes in Molecular Systems*, Singapore: World Scientific, 1996.

62 S. M. Cybulski, R. A. Kendall, G. Chalasinski, M. W. Severson and M. M. Szczesniak, *The Journal of Chemical Physics*, 1997, **106**, 7731–7737.

63 F. Y. Naumkin and F. R. W. Mccourt, *Molecular Physics*, 2004, **102**, 37–45.

64 X.-G. Wang and T. Carrington, *The Journal of Chemical Physics*, 2019, **151**, 054101.

65 I. S. Ulusoy, D. A. Andrienko, I. D. Boyd and R. Hernandez, *The Journal of Chemical Physics*, 2016, **144**, 234311.

66 J. Hellemans, J. Kestin and S. Ro, *Physica*, 1973, **65**, 362–375.

67 E. A. Mason, *The Journal of Chemical Physics*, 1955, **23**, 49–56.

68 C. L. Kong and M. R. Chakrabarty, *The Journal of Physical Chemistry*, 1973, **77**, 2668—-2670.

69 A. E. Sherwood and J. M. Prausnitz, *The Journal of Chemical Physics*, 1964, **41**, 429–437.

70 W. Hogervorst, *Physica*, 1971, **51**, 77–89.

71 J. O. Hirsehfelder, C. F. Curtiss and R. B. Bird, *Molecular theory of gases and liquids, Chap. 6*, John Wiley and Sons, New York, 1954, p. 1249.

72 P. Foreman, A. Lees and P. Rol, *Chemical Physics*, 1976, **12**, 213–224.

73 S. M. Cybulski, R. Burcl, G. Chalasinski and M. M. Szczesniak, *The Journal of Chemical Physics*, 1995, **103**, 10116–10127.

74 B. P. Reid, K. C. Janda and N. Halberstadt, *The Journal of Physical Chemistry*, 1988, **92**, 587—-593.

75 P. J. Knowles, C. Hampel and H. Werner, *The Journal of Chemical Physics*, 1993, **99**, 5219–5227.

76 M. J. Deegan and P. J. Knowles, *Chemical Physics Letters*, 1994, **227**, 321–326.

77 C. Amiot and J. Verges, *Can. J., Phys*, 1981, **59**, l98l.

78 G. Knizia, T. B. Adler and H.-J. Werner, *The Journal of chemical physics*, 2009, **130**, 054104.

79 K. A. Peterson, T. B. Adler and H.-J. Werner, *The Journal of chemical physics*, 2008, **128**, 084102.

80 D. Feller, K. A. Peterson and T. D. Crawford, *The Journal of chemical physics*, 2006, **124**, 054107.

81 H. Werner, P. Knowles, G. Knizia, F. Manby, M. Schütz, P. Celani, W. Györffy, D. Kats, T. Korona, R. Lindh *et al.*, *MOLPRO, version 2019.1, a package of ab initio programs*, University College Cardiff Consultants Ltd.: Cardiff, UK, 2019.

82 R. Dawes, X.-G. Wang and T. Carrington Jr, *The Journal of Physical Chemistry A*, 2013, **117**, 7612–7630.

83 E. Quintas-Sánchez, R. Dawes, K. Lee and M. C. McCarthy, *The Journal of Physical Chemistry A*, 2020.

84 M. C. McCarthy, S. A. Ndengué and R. Dawes, *The Journal of Chemical Physics*, 2018, **149**, 134308.

85 M. B. Khalifa, E. Quintas-Sánchez, R. Dawes, K. Hammami and L. Wiesenfeld, *Physical Chemistry Chemical Physics*, 2020, **22**, 17494–17502.

86 A. Faure, P. J. Dagdigian, C. Rist, R. Dawes, E. Quintas-Sánchez, F. Lique and M. Hochlaf, *ACS Earth and Space Chemistry*, 2019, **3**, 964–972.

87 C. T. Bop, F. A. Batista-Romero, A. Faure, E. Quintas-

Sánchez, R. Dawes and F. Lique, *ACS Earth and Space Chemistry*, 2019, **3**, 1151–1157.

88 E. Quintas-Sánchez and R. Dawes, *J. Chem. Inf. Model.*, 2019, **59**, 262–271.

89 R. Dawes and E. Quintas-Sánchez, *Reviews in Computational Chemistry vol. 31*, Wiley, 2018, ch. 5, pp. 199–264.

90 R. Dawes, X.-G. Wang, A. W. Jasper and T. Carrington Jr, *The Journal of chemical physics*, 2010, **133**, 134304.

91 M. Majumder, S. A. Ndengué and R. Dawes, *Molecular Physics*, 2016, **114**, 1–18.

92 M. Mizushima *et al.*, *Theory of rotating diatomic molecules*, Wiley, 1975.

93 W. Gordy and R. L. Cook, *Microwave molecular spectra*, Wiley,, 1984.

94 F. Lique, A. Spielfiedel, M.-L. Dubernet and N. Feautrier, *The Journal of chemical physics*, 2005, **123**, 134316.

95 S. Ndengué, R. Dawes, X.-G. Wang, T. Carrington Jr, Z. Sun and H. Guo, *The Journal of chemical physics*, 2016, **144**, 074302.

96 J. Hutson and S. Green, *Swindon, UK*, 1994.

97 M. H. Alexander and D. E. Manolopoulos, *The Journal of chemical physics*, 1987, **86**, 2044–2050.

98 F. Lique, *The Journal of Chemical Physics*, 2010, **132**, 044311.